AIR POLLUTION OVER NORTH-WEST BAY OF BENGAL IN THE EARLY POST-MONSOON SEASON BASED ON NASA MERRAERO DATA

Pavel Kishcha,

Department of Geophysical, Atmospheric and Planetary Sciences, Tel-Aviv University, 69978 Tel-Aviv, Israel

Arlindo M. da Silva

Global Modeling and Assimilation Office, NASA/GSFC, Greenbelt, Maryland USA.

Boris Starobinets

Department of Geophysical, Atmospheric and Planetary Sciences, Tel-Aviv University, 69978 Tel-Aviv, Israel

Pinhas Alpert

Department of Geophysical, Atmospheric and Planetary Sciences, Tel-Aviv University, 69978 Tel-Aviv, Israel

Journal of Geophysical Research – Atmospheres,

Submitted in June 2013

Abstract

The MERRA Aerosol Reanalysis (MERRAero) has been recently developed at NASA's Global Modeling Assimilation Office (GMAO). This reanalysis is based on a version of the GEOS-5 model radiatively coupled with GOCART aerosols, and it includes assimilation of bias-corrected Aerosol Optical Thickness (AOT) from the MODIS sensor on both Terra and Aqua satellites. Our main finding is that, in October, in the absence of aerosol sources in north-west Bay of Bengal (BoB), MERRAero showed increasing AOT trends over north-west BoB exceeding those over the east of the Ganges basin. The Ganges basin is characterized by significant population growth accompanied by developing industry, agriculture, and increasing transportation: this has resulted in declining air quality. MERRAero data for the period 2002-2009 was used to study AOT trends over north-west Bay of Bengal (BoB) in the early post-monsoon season. This season is characterized by aerosol transport from the Ganges basin to north-west BoB by prevailing winds; and still significant rainfall of over 150 mm/month. Different aerosol components showed strong increasing AOT trends over north-west BoB. The following factors contributed to the increasing AOT trend over the area in question in October: an increasing number of days when prevailing winds blew from land to sea, resulting in a drier environment and an increase in air pollution over north-west BoB; wind convergence was observed over north-west BoB causing the accumulation of aerosol particles over that region, when prevailing winds blew from land to sea. MERRAero aerosol reanalysis can be used on a global scale.

1. Introduction

The Indian subcontinent (and the Ganges basin in particular) is characterized by a significant population growth accompanied by developing industry, agriculture, and increasing transportation. This has resulted in declining air quality [Di Girolamo et al. 2004, Ramanathan and Ramana, 2005, Tripathi et al., 2005, Prasad and Singh, 2007, Kaskaoutis et al., 2011a, Dey and Di Girolamo, 2011, Krishna Moorthy et al., 2013]. With respect to air pollution, one could suggest some relationship between population figures and anthropogenic aerosol emissions. Indeed, Kishcha et al. [2011] showed that, over extensive areas with differing population densities in the Indian subcontinent, the higher the averaged population density – the larger the averaged AOT. In addition, the larger the population growth - the stronger the increasing AOT trends.

Prevailing winds blowing along the Ganges basin in the post-monsoon and winter months transport anthropogenic aerosol particles into the Bay of Bengal (BoB) [Di Girolamo et al. 2004, Prasad and Singh, 2007, Kumar et al., 2010]. The resulting increased levels of air pollution over BoB were investigated during a number of sea expeditions [Ramachandran and Jayaraman, 2003; Vinoj et al., 2004; Ganguly et al., 2005, Moorthy et al., 2008, Kumar et al., 2010, Kaskaoutis et al., 2011b]. Moreover, long-term AOT trends over South Asia, including BoB, were examined, using different satellite AOT data sets, by Mishchenko and Geogdzhayev [2007], Zhao et al. [2008], Zhang and Reid [2010], Kaskaoutis et al. [2011a], Dey and Di Girolamo [2011], and Hsu et al. [2012]. Based on AVHRR satellite data, Mishchenko and Geogdzhayev [2007] compared over-water AOT averaged over two separate periods, 1988–1991 and 2002–2005, and found significant changes. Zhao et al. [2008] studied AOT trends over the whole area of BoB for spring, summer, autumn, and winter during the 25-year period 1981 – 2005, using AVHRR data. Using MODIS-Terra Level 2 AOT data, Zhang and Reid [2010] analyzed AOT trends over the whole area of BoB for all months during the 10-year period 2000 - 2009. The spatial distribution of decadal (2000 – 2009) MODIS Level-3 AOT trends over South Asia, including BoB, in different months was obtained by Kaskaoutis et al. [2011a]. Using MISR aerosol data, decadal (2000 – 2009) AOT trends over the Indian subcontinent and surrounding sea areas were also estimated by Dey and Di Girolamo [2011]. Hsu et al. [2012] created maps of SeaWiFS AOT trends over the period 1998 – 2010 for each of the four seasons. In the aforementioned studies, however, specific features of AOT trends over north-west BoB in the early post-monsoon season were not discussed.

The early post-monsoon season over the study region is characterized by aerosol transport from the Ganges basin to north-west BoB by prevailing winds; and still significant rainfall of over 150 mm/month over the east of the Ganges basin and north-west BoB. It would be reasonable to consider that AOT trends over sea areas in BoB were created by changes in aerosol sources on the land in the Indian subcontinent. In our previous study [Kishcha et al., 2012], we found that it was not always the case. Specifically, we found that, in October, MODIS showed strong increasing aerosol optical thickness (AOT) trends over north-west Bay of Bengal (BoB) in the absence of AOT trends over the east of the Indian subcontinent. This was unexpected, because sources of anthropogenic pollution were located over the Indian subcontinent, mainly in the Ganges basin, and aerosol transport from the Indian subcontinent to north-west BoB was carried out by prevailing winds.

It was interesting to determine whether existing state-of-the-art aerosol data-assimilated systems were capable of reproducing the aforementioned observed AOT trends over north-west BoB, in the early post-monsoon season, in the presence of significant rainfall. For the model, it would be a challenge just to obtain correct space-time distribution of rainfall, which is of importance for estimating aerosol wet removal. The NASA Goddard Earth Observing System (GEOS-5) was used to extend the NASA Modern Era-Retrospective Analysis for Research and Applications (MERRA) reanalysis by adding five atmospheric aerosol components (sulfates, organic carbon, black carbon, desert dust, and sea-salt). In the current study, the obtained eight-year (2002 – 2009) assimilated aerosol dataset (so-called MERRAero) was applied to examine aerosol trends over north-west Bay of Bengal (BoB) in the post-monsoon season. Using an assimilated aerosol dataset over north-west BoB provided us with an opportunity to estimate the contribution of different aerosol components to AOT and its trends. It is worth noting that only AOT was assimilated by GEOS-5, while details of the aerosol specificion are to a large extent dependent on emission inventories assumed by the model.

2. GEOS-5 and the MERRA Aerosol Reanalysis (MERRAero)

2.1 GEOS-5 Earth Modeling System

GEOS-5 is the latest version of the NASA Global Modeling and Assimilation Office (GMAO) Earth system model. GEOS-5 contains components for atmospheric circulation and composition (including atmospheric data assimilation), ocean circulation and biogeochemistry, and land surface processes. Components and individual parameterizations within components are coupled under the Earth System Modeling Framework (ESMF) [Hill et al., 2004]. In addition to traditional meteorological parameters (winds, temperatures, etc. [Rienecker et al., 2008]), GEOS-5 includes modules representing the atmospheric composition, most notably aerosols [Colarco et al., 2010], and tropospheric/stratospheric chemical constituents [Pawson et al., 2008], and the impact of these constituents on the radiative processes of the atmosphere.

2.2 Aerosols in GEOS-5

GEOS-5 includes modules representing atmospheric composition, including aerosols [Colarco et al., 2010] and tropospheric and stratospheric chemical constituents [Pawson et al., 2008]. The current generation aerosol module is based on a version of the Goddard Chemistry, Aerosol, Radiation, and Transport (GOCART) model [Chin et al., 2002]. GOCART treats the sources, sinks, and chemistry of dust, sulfate, sea salt, and black and organic carbon aerosols. Aerosol species are assumed to be external mixtures. Aerosol emissions are based on the AeroCom version 2 hindcast inventories [Dr. Thomas Diehl, personal communication, and http://aerocom.met.no/emissions.html). Total mass of sulfate and carbonaceous aerosols are tracked, while for dust and sea salt the particle size distribution is explicitly resolved across five non-interacting size bins for each. Both dust and sea salt have wind-speed dependent emission functions, while sulfate and carbonaceous species have emissions principally from fossil fuel combustion, biomass burning, and bio-fuel consumption, with additional biogenic sources of organic carbon. Sulfate has additional chemical production from oxidation of SO2 and dimethylsulfide (DMS), as well as a database of volcanic SO2 emissions and injection heights.

For all aerosol species, optical properties are primarily from the commonly used Optical Properties of Aerosols and Clouds (OPAC) data set [Hess et al., 1998]. OPAC provides the spectrally varying refractive index and a humidification factor for each aerosol species which, together with assumptions about the particle size distribution of each species, are used to construct spectrally varying lookup tables of aerosol optical properties such as the mass extinction efficiency, single scattering albedo, and asymmetry parameter, inputs required by our radiative transfer codes (details are in Colarco et al. [2010], and references therein). Daily biomass burning emissions are from the Quick Fire Emission Dataset (QFED) and are derived from MODIS fire radiative power retrievals [Darmenov and da Silva, 2013].

2.3 GEOS-5 Data Assimilation

GEOS-5 has a mature atmospheric data assimilation system that builds upon the Grid-point Statistical Interpolation (GSI) algorithm, jointly developed with NCEP [Wu et al. 2002, Derber et al. 2003, Rienecker et al. 2008]. The GSI solver was originally developed at NCEP as an unified 3D-Var analysis system for supporting global and regional models. GSI includes all the in-situ and remotely sensed data used for operational weather prediction at NCEP.

GEOS-5 also includes assimilation of AOT observations from the MODIS sensor on both Terra and Aqua satellites. Based on the work of Zhang and Reid [2006] and Lary [2009], a back-propagation neural network has been developed to correct observational biases related to cloud contamination, surface parameterization, aerosol microphysics, etc. On-line quality control is performed with the adaptive buddy check of Dee et al. [2001], with observation and background errors estimated using the maximum likelihood approach of Dee and da Silva [1999]. The AOT analysis in GEOS-5 is performed by means of analysis splitting. First, a 2D analysis of AOT is performed using error covariances, derived from innovation data. The 3D analysis increments of aerosol mass concentration are computed using an ensemble formulation for the background error covariance. In MERRAero, as well as in the GEOS-5 near real-time system, this calculation is performed using the Local Displacement Ensemble (LDE) methodology under the assumption that ensemble perturbations are meant to represent misplacements of the aerosol plumes. These ensemble perturbations are generated with full model resolution, without the need for multiple model runs.

2.4 MERRA Aerosol (MERRAero) Reanalysis

MERRA is a NASA reanalysis for the satellite era using a major new version of the Goddard Earth Observing System Data Assimilation System Version 5 (GEOS-5). The Project focuses on historical analyses of the hydrological cycle from the NASA EOS suite of observations in a climate context, on a broad range of weather and climate time scales and places. The MERRA time period covers the modern era of remotely sensed data, from 1979 through the present, and the special focus of the atmospheric assimilation is the hydrological cycle. Like other similar reanalysis, MERRA provides meteorological parameters (winds, temperature, humidity), along with a number of other diagnostics such as surface and top of the atmosphere fluxes, diabatic terms and the observational corrections imposed by the data assimilation procedure.

As a step toward an Integrated Earth System Analysis (IESA), the GMAO is producing several parallel re-analyses of other components of the earth system such as ocean, land and atmospheric composition. Of particular relevance for this paper the MERA Aerosol Reanalysis (MERRAero), where MODIS AOT observations are assimilated providing a companion aerosol gridded datasets that can be used to study the impact of aerosols on the atmospheric circulation and on air quality in general. Table 1 summarizes the main attributes of MERRAero. Notice that MERRAero only covers the later years of MERRA, capitalizing on the improved aerosol measurements from NASA's EOS platforms.

3. Method

Following our previous study [Kishcha et al., 2012], we analyzed long-term variations of AOT over seven zones, each 3^o x 3^o, located in the Ganges basin and north-west BoB (Fig. 1). As mentioned, in the post-monsoon period, prevailing winds blow along the Ganges basin. The specified zones in the Ganges basin provide us with an opportunity for analyzing air pollution trends produced by local sources and aerosol transport. Fig. 1a shows the spatial distribution of eight-year mean MERRAero AOT over the region under consideration in October, together with the location of zones 3^o x 3^o in the Indian subcontinent (zone 1 to zone 5) and in the Bay of Bengal (zones 6 and 7). MERRAero monthly AOT data are available from the year 2002. To analyze AOT and its trends over the Indian subcontinent and north-west BoB, we used monthly MERRAero AOT data with horizontal resolution of approximately 50 km, during the eight-year period 2002 – 2009.

A linear fit was used to determine the resulting trend of aerosol optical thickness during the study period (2002 – 2009) over each of the aforementioned zones. The obtained AOT trend values correspond to the slope of the linear fit. To ensure that the linear fit produced normally distributed residuals, they were required to pass the Shapiro–Wilk normality test [Shapiro and Wilk, 1965, Razali and Wah, 2011]. If the residuals were normally distributed, they could be used in a t-test, in order to estimate the statistical significance of a linear fit. The statistical significance of the AOT trend was checked by applying the significance level (p) value, i.e. $p < 0.05$ for statistically significant AOT trends at the 95 % confidence level.

4. Results

4.1. Comparison between total MERRAero and MODIS AOT trends in October

In accordance with space distribution of eight-year mean AOT in the early post-monsoon season (October), MERRAero showed high AOT values over the Ganges basin with a maximum over the north-west part of the Ganges basin (Fig. 1a). Therefore, MERRAero data were able to reproduce the main structure of aerosol distribution over the Ganges basin. The Ganges basin is the most polluted part of the Indian subcontinent, where highly-populated areas and main industrial centers are located.

We analyzed zone-to-zone variations of MERRAero AOT averaged over the specified zones. In the early post-monsoon season (October), MERRAero showed mainly decreasing AOT variations from zone 3 to zone 5 (Fig. 2a and Table 2). Note that this decrease in AOT from north-west to east of the Ganges basin does not correspond to the distribution of population density: population density is higher in the east of the Ganges basin (zones 4 and 5) than in the north-west of the Ganges basin (zone 1) (Fig. 3). At first glance, this is contradictory to our previous findings on the relationship between AOT and population density in the Indian subcontinent [Kishcha et al., 2011]. It should be mentioned, however, that, in our previous study, we used averaging over significant areas of the Indian subcontinent with differing population densities.

The most probable reason for the decrease in AOT over the east of the Ganges basin, where population density is the highest in the Ganges basin, is wet removal processes after significant rainfall in October. Monthly accumulated Tropical Rainfall Measuring Mission (TRMM) rainfall data from the 3B42V6 archive, on a 0.25º × 0.25º latitude-longitude grid [Huffman et al., 2007], were used to estimate zone-to-zone variations of eight-year (2002 – 2009) mean TRMM rainfall over the specified zones in October (Fig. 4). High rainfall values of over 150 mm can be seen in October over the east of the Ganges basin (zone 5) and north-west BoB (zone 6). Moreover, rainfall data showed that, over the east of the Ganges basin, the accumulated rainfall in October in the first four-year period 2002 – 2005 was essentially higher than in the second four-year period 2006 – 2009 (Fig. 4). As a result, higher values of MERRAero AOT over the east of the Ganges basin (zones 4 and 5) were observed in the second four-year period 2006 – 2009 than in the first four-year period 2002 – 2005 (Fig. 2b).

Space distributions of MERRAero AOT trends during the eight-year (2002 – 2009) study period showed strong increasing AOT trends over north-west BoB exceeding those over the Ganges basin (Fig. 1b). This indicates that MERRAero is capable of reproducing the main features of the phenomenon of strong increasing AOT trends over north-west BoB in the early post-monsoon season, in line with our previous study [Kishcha et al., 2012].

4.2. Effects of rainfall on MERRAero AOT

As mentioned, in the early post-monsoon season (October), intense rainfall can be frequently observed over the east of the Ganges basin. These severe precipitation events could strongly affect AOT over the east of the Ganges basin due to aerosol wet removal processes. To understand the rain effects on AOT over the east of the Ganges basin (zone 5), we compared year-to-year variations of assimilated MERRAero AOT and TRMM accumulated rainfall, over zone 5 in each October during the study period (Fig. 5a). Rainfall data showed that the accumulated rainfall in October in the first four-year period 2002-2005 was higher than in the second four-year period 2006-2009 (Fig. 5a). A strong inverse negative relationship (with a high negative correlation of over -0.8) between changes in assimilated MERRAero AOT and rainfall is clearly seen: each increase in rainfall was accompanied by a decrease in assimilated AOT (Fig. 5a). The aforementioned decrease in rainfall over zone 5 in October during the study period can explain some increasing trend in MERRAero AOT observed over that area in October (Fig. 5a and Table 2). There was some dissimilarity in the rainfall amount between the east of the Ganges basin (zone 5) and north-west BoB (zone 6): Fig. 5b does not show as clear decreasing trends in rainfall amount over north-west BoB as over the east of the Ganges basin in Fig. 5a.

4.3. AOT of different aerosol species and their trends in the early post-monsoon season

As known, satellite remote sensing data can not distinguish between different aerosol species. MERRAero provides us with an opportunity to investigate the contribution of different aerosol components to AOT and its trends. Based on MERRAero model data, Fig. 6a represents zone-to-zone variations of eight-year (2002 – 2009) mean AOT of several aerosol components (desert dust; organic and black carbon; and sulfates) averaged over specified zones in October, and their trends. One can see that, over zone 1, there was a considerable amount of carbon aerosols (as a result of crop waste burning [Sharma et al., 2010]), dust particles, and sulfate aerosols (Fig. 6a). This explains the AOT maximum over the north-west of the Ganges basin in October.

By contrast to sulfates and carbonates, dust aerosol particles have no sources along the Ganges basin. Therefore, dust distribution along the Ganges basin is determined by aerosol transport (by the action of prevailing winds blowing along the Ganges basin) and by deposition processes. One can see that the eight-year mean dust AOT values noticeably decreased along the Ganges basin and over north-west BoB. This resulted in the decrease in dust contribution to the total AOT from approximately 30% over zone 1 to 8% over zones from 5 to 7 (Table 3). Furthermore, dust AOT trends did not change in transition from land to sea: approximately the same slightly increasing dust AOT trends of ~0.004 yr-1 were obtained along the east of the Ganges basin and over north-west BoB (Fig. 6b). We found that these AOT trends over zones from 5 to 7 were statistically significant (Table 3). The same dust AOT trends along the Ganges basin and over north-west BoB suggest an increasing trend in some external source of dust emissions, outside the Ganges basin. It should be kept in mind that MERRAero only assimilates total AOT and that the trend in aerosol speciation may depend on the trend (or lack thereof) of the specified emissions.

The distribution of sulfate AOT along the Ganges basin is determined by sulfate aerosol emissions, together with aerosol transport (by the action of prevailing winds) and deposition processes (Fig. 6a). The sulfate contribution to the total AOT increased along the Ganges basin from approximately 30 % over zone 1 to ~56% over zone 5 (Table 3). Over north-west BoB (zones 6 and 7), the sulfate contribution to the total AOT was over 50% (Table 3). Thus, according to MERRAero AOT data, sulfates were the major atmospheric aerosol component over the east of the Ganges basin and over north-west BoB. Moreover, MERRAero data showed that sulfate AOT trends changed in transition from land to sea: strong statistically-significant increasing sulfate AOT trends (of 0.008 yr^{-1} and 0.011 yr^{-1} over zones 6 and 7 respectively) exceeded those over the east of the Ganges basin (zone 5) (Fig. 6b, and Table 3).

With respect to organic and black carbon aerosols, their distribution of eight-year mean AOT values along the Ganges showed a wide maximum from the north-west to the center of the Ganges basin (zones from 1 to 3) (Fig. 6a). This area of maximum carbon AOT is known for crop waste burning aerosols [Sharma et al., 2010. Venkataraman et al., 2006]. AOT values of carbon aerosols decrease to the east from zone 3 (Fig. 6a). As discussed in Section 4.1, the reason for the decrease in AOT over the east of the Ganges basin in October is significant rainfall accompanied by aerosol wet removal processes. The joint contribution of organic and black carbon aerosols to the total AOT is ~38% over the north-west of the Ganges basin (zones from 1 to 3); ~35% over the east of the Ganges basin (zone 5), and approximately 27% over north-west BoB (zones 6 and 7) (Table 3). Similar to AOT trends of sulfate aerosols, MERRAero showed that AOT trends of carbon aerosols changed in transition from land to sea: increasing AOT trends in organic and black carbon AOT over the sea (zones 6 and 7) exceeded those over zone 5 in the land (Fig. 6b, and Table 3).

Based on MERRAero data, we found that, in October, the contribution of sea-salt aerosols to the total AOT over the east of the Ganges basin and north-west BoB was even lower than that of desert dust. Therefore, over the east of the Ganges basin and north-west BoB in October, anthropogenic aerosols dominate natural aerosols (Table 3).

4.4. Factors contributing to AOT trends over north-west BoB

MERRAero showed increasing AOT trends over north-west BoB in October exceeding AOT trends over the east of the Ganges basin (Fig. 1b). This was despite the fact that sources of air pollution are located on the land, mainly in the Ganges basin. There could be several factors contributing to the increasing AOT trends over north-west BoB. First, there were changes in the atmospheric circulation over north-west BoB in October during the eight-year study period (Fig. 7). Mean wind vectors of the 700-850 hPa layer in each October during the 8-year period under consideration were analyzed (Fig. 7). The 700-850 hPa layer is considered as indicative of wind in the lower troposphere, where aerosol transport mainly occurs [Dunion and Velden, 2004]. During the second 4-year period (2006 – 2009), prevailing winds blowing mainly from land to sea (Fig. 7, e - h) resulted in a drier environment and less precipitation over the east of the Ganges basin and north-west BoB (Fig. 4) than during the first 4-year period (2002 – 2005) (Fig. 7, a - d). This caused less wet removal of air pollution in the second 4-year period than in the first 4-year period. Second, our analysis showed that, during the eight-year study period, there was an increasing number of days (Np, in percentage form) in each October when prevailing winds blew from land to sea (Fig. 8). This suggests some increasing trends in the transport of anthropogenic air pollution from their sources in the east of the Ganges basin to north-west BoB. Third, for Octobers when Np > 50%, wind convergence was observed over north-west BoB causing the accumulation of aerosol particles over that region (Fig. 9), in line with our previous study [Kishcha et al., 2012]. All the three factors contributed to the increasing AOT trend over north-west BoB in the early post-monsoon season.

During the second 4-year period (2006 – 2009), a decrease in atmospheric humidity was observed. We analyzed observations of atmospheric relative humidity from the AIRS (Atmospheric Infrared Sounder) instrument aboard the NASA's Aqua satellite, available from 2002 [Fasullo and Trenberth, 2012]. Fig. 10a represents year-to-year variations of relative humidity (RH) of the 700-850 hPa layer over north-west BoB in each October during the study period 2002 - 2009, taken on the ascending node of the Aqua satellite orbit (on the day side of the Earth). Quite noticeable non-linear decreasing RH trends can be clearly seen over north-west BoB (zones 6 and 7) during the study period. MERRA reanalysis (used as a driver for the GEOS-5 model in order to obtain MERRAero aerosol data set) was capable of reproducing the aforementioned observed changes in relative humidity over north-west BoB (Fig. 10b).

The aforementioned decrease in relative humidity over north-west BoB during the study period was accompanied by a decrease in the effective size of hygroscopic aerosol particles. This process contributed to a decrease in AOT of hygroscopic aerosols [Bian et al., 2009]. One could expect to get a direct relationship between AOT and RH: an increase in RH should lead to an increase in AOT. However, MERRAero showed an inverse relationship between AOT and RH: a decrease in RH over north-west BoB in October was accompanied by an increase in AOT (Fig. 11). This is evidence that other factors, affecting AOT, were more effective than the decrease in AOT due to the decrease in effective size of hygroscopic aerosol particles.

Consequently, there were competing processes affecting AOT over north-west BoB in the early post-monsoon season. MERRAero showed that these competing processes resulted in increasing AOT trends over north-west BoB exceeding those over the east of the Ganges basin.

5. Conclusions

The recently developed eight-year (2002 – 2009) MERRAero assimilated aerosol dataset was applied to the study of AOT and its trends over north-west BoB in the early post-monsoon season. Our main finding is that, in October, in the absence of aerosol sources in north-west BoB, MERRAero showed increasing AOT trends over north-west BoB exceeding those over the east of the Ganges basin. Different aerosol components showed strong increasing AOT trends over north-west BoB.

There were a number of factors contributing to the increasing AOT trend over the area in question:

- an increasing number of days in each October when prevailing winds blew from land to sea, resulting in an increase in air pollution over north-west BoB;

- during the second 4-year period (2006 – 2009), prevailing winds blowing mainly from land to sea were responsible for a drier environment with less precipitation causing less wet removal of air pollution than in the first 4-year period (2002 – 2005);
- in each October, when prevailing winds blew from land to sea, wind convergence was observed over north-west BoB causing the accumulation of aerosol particles over that region, in line with our previous study [Kishcha et al., 2012].

Over the region under consideration, MERRAero showed the main structure of space distribution of AOT in October, averaged over the study period: high AOT values over the Ganges basin with a maximum over the north-west of the Ganges basin. The MERRAero AOT data set allowed us to determine the causal factor for this AOT maximum, which is a considerable amount of carbon aerosols (from bio-mass burning), dust particles, and sulfates. Over north-west BoB in the early post-monsoon season, MERRAero showed that aerosols were dominated by anthropogenic air pollution, such as sulfates and carbon aerosols.

MERRAero aerosol reanalysis can be used on a global scale for analyzing AOT of different aerosol species.

References

Bian, H., M. Chin, J. Rodriguez, H. Yu, J. Penner, and S. Strahan (2009), Sensitivity of aerosol optical thickness and aerosol direct radiative effect to relative humidity. *Atmos. Chem. Phys*, 9, 2375 – 2386, doi:10.5194/acp-9-2375-2009.

Chin, M., P. Ginoux, S. Kinne, O. Torres, B. Holben, B.N. Duncan, R.V. Martin, J. Logan, A. Higurashi, T. Nakajima (2002), Tropospheric aerosol optical thickness from the GOCART model and comparisons with satellite and sun photometer measurements. *J. Atmos. Phys*. 59, 461–483, doi: http://dx.doi.org/10.1175/1520-0469(2002)059.

Colarco, P., A. da Silva, M. Chin, and T. Diehl (2010), Online simulations of global aerosol distributions in the NASA GEOS-4 model and comparisons to datellite and ground-based aerosol optical depth. *J. Geophys. Res*., 115, D14207, doi:10.1029/2009JD012820.

Darmenov, A., and A.M. da Silva (2013), The quick fire emissions dataset (QFED) - Documentation of versions 2.1, 2.2 and 2.4. NASA Technical Report Series on Global Modeling and Data Assimilation. NASA TM-2013-104606, 32, 183p.

Dee, D.P., L. Rukhovets, R. Todling, A.M. da Silva, and J.W. Larson (2001), An Adaptive Buddy Check for Observational Quality Control. *Quarterly Journal of the Royal Meteorological Society,* 127(577), 2451–2471, doi:10.1002/qj.49712757714.

Dee, D.P., and A.M. da Silva (1999), Maximum-Likelihood Estimation of Forecast and Observation Error Covariance Parameters. Part I: Methodology. *Mon. Weather Rev.*, 127(8), 1822–1834, doi:http://dx.doi.org/10.1175/1520-0493.

Derber, J. C., R.J. Purser, W.-S. Wu, R. Treadon, M. Pondeca, D. Parrish, and D. Kleist (2003), Flow-dependent Jb in a global grid-point 3D-Var. *Proc. ECMWF annual seminar on recent developments in data assimilation for atmosphere and ocean.* Reading, UK, 8-12 Sept. 2003.

Dey, S., and L. Di Girolamo (2011), A decade of change in aerosol properties over the Indian subcontinent, *Geophys. Res. Lett.,* 38, L14811, doi:10.1029/2011GL048153.

DI Girolamo, L., T.C. Bond, D. Bramer, D.J. Diner, F. Fettinger, R.A. Kahn, J.V. Matronchik, M.V. Ramanathan, and P.J. Rash (2004), Analysis of Multi-angle Imaging SpectroRadiometer (MISR) aerosol optical depths over greater India during winter 2001 – 2004. *Geophys. Res. Lett.*, 31, L23115, doi:10.1029/2004GL021273.

Dunion, J. P., and C. S. Velden (2004), The impact of the Saharan air layer on Atlantic tropical cyclone activity, *Bull. Am. Meteorol. Soc*., 85(3), 353– 365, doi:10.1175/BAMS-85-3-353.

Fasullo, J., and K. Trenberth (2012). A less cloudy future: the role of subtropical subsidence in climate sensitivity, *Science*, 338, 792-794.

Ganguly, D., A. Jayaraman, and H. Gadhavi (2005), In situ ship cruise measurements of mass concentration and size distribution of aerosols over Bay of Bengal and their radiative impacts. *J. Geophys. Res*., 110, D06205, doi:10.1029/2004JD005325.

Hill, C, C. DeLuca, Balaji, M. Suarez, and A. da Silva (2004): The architecture of the Earth System Modeling Framework. *Computing in Science and Engineering*, 6(1), 18–28.

Hsu, N.C., R. Gautam, A.M. Sayer, C. Bettenhausen, C. Li, M.J. Jeong, S.C. Tsay, and B.N. Holben (2012), Global and regional trends of aerosol optical depth over land and ocean using SeaWiFS measurements from 1997 to 2010. *Atmos. Chem. Phys. Discuss*., 12, 8465-8501, doi:10.5194/acpd-12-8465-2012.

Huffman, G.J., R.F. Adler, D.T. Bolvin, G. Gu, E.J. Nelkin, K.P. Bowman, Y. Hong, E.F. Stocker, D.B. Wolff (2007), The TRMM multisatellite precipitation analysis (TMPA): quasi-global, multiyear, combined-sensor precipitation estimates at fine scales. *J. Hydrometeorology*, 8, 38 – 55, doi: 10.1175/JHM560.1.

Kaskaoutis, D.G., S.K. Kharol, P.R. Sinha, R.P. Singh, K.V.S. Badarinath, W. Mehdi, and M. Sharma (2011a). Contrasting aerosol trends over South Asia during the last decade based on MODIS observations. *Atmos. Meas. Tech. Discuss*., 4, 5275–5323, doi:10.5194/amtd-4-5275-2011.

Kaskaoutis, D.G., S. Kumar Kharol, P.R. Sinha, R.P. Singh, H.D. Kambezidis, A. Rani Sharma, and K.V.S. Badarinath (2011b), Extremely large anthropogenic aerosol contribution to total aerosol load over the Bay of Bengal during winter season. *Atmos. Chem. Phys.,* 11, 7097–10 7117, doi:10.5194/acp-11-7097-2011.

Kishcha, P., B. Starobinets, O. Kalashnikova, and P. Alpert (2011), Aerosol optical thickness trends and population growth in the Indian subcontinent. *Int. J. Remote. Sens.,* 32, 9137-9149, doi:10.1080/01431161.2010.550333.

Kishcha, P., B. Starobinets, C.N. Long, P. Alpert (2012), Unexpected increasing AOT trends over north-west Bay of Bengal in the early post-monsoon season. *J. Geophys. Res*., 117, D23208, doi 10.1029/2012JD018726.

Krishna Moorthy, K., S. Suresh Babu, M.R. Manoj, and S.K. Satheesh (2013), Buildup of aerosols over the Indian region. *Geophys. Res. Lett*., doi:10.1002/GRL.50165.

Kumar, A., M.M. Sarin, and B. Srinivas (2010), Aerosol iron solubility over Bay of Bengal: Role of anthropogenic sources and chemical processing, *Marine Chemistry*, 121, 167–175.

Lary, D.J., L.A. Remer, D. MacNeill, B. Roscoe, and S Paradise (2009), Machine Learning and Bias Correction of MODIS Aerosol Optical Depth. *Geoscience and Remote Sensing Letters*, IEEE, 6(4), 694–698, doi: 10.1109/LGRS.2009.2023605.

Mishchenko, M. I., and I. V. Geogdzhayev (2007), Satellite remote sensing reveals regional tropospheric aerosol trends, Opt. Express, 15, 7423 – 7438, doi:10.1364/OE.15.007423.

Moorthy, K.K., S.K. Satheesh, S.S. Babu, and C.B.S. Dutt (2008), Integrated campaign for aerosols, gases and radiation budget (ICARB): An overview. *J. Earth Syst. Sci*., 117, 243–262, doi:10.1007/s12040-008-0029-7.

Pawson, S., R.S Stolarski, A.R. Douglass, P.A. Newman, J.E.c Nielsen, S.M. Frith, and M.L Gupta (2008), Goddard Earth Observing System Chemistry-Climate Model Simulations of Stratospheric Ozone-Temperature Coupling Between 1950 and 2005. *J. Geophys. Res.*, 113(D12), D12103, doi:10.1029/2007JD009511.

Prasad, A.K. and R.P. Singh (2007), Comparison of MISR-MODIS aerosol optical depth over the Indo-Gangetic basin during the winter and summer seasons (2000-2005). *Remote Sensing of Environment*, 107, 109 – 119, doi:10.1016/j.rse.2006.09.026.

Ramachandran, S. and A. Jayaraman (2003), Spectral aerosol optical depths over Bay of Bengal and Chennai: II – Sources, anthropogenic influence and model estimates. *Atmos. Env.,* 37, 1951–1962, doi:10.1016/S1352-2310(03)00082-7.

Ramanathan, V., and M. Ramana (2005), Persistent, widespread and strongly absorbing haze over the Himalayan foothills and the Indo-Gangetic plains. *Pure and Applied Geophysics*, 162, 1609 – 1626, doi:10.1007/s00024-005-2685-8.

Razali, N.M., and Y.B. Wah (2011), Power comparisons of Shapiro-Wilks, Kolmogorov-Smirnov, Lilliefors and Anderson-Darling tests. *J. Statistical Modeling and Analytics,* 2, 21-33.

Rienecker, MM, MJ Suarez, R Todling, J Bacmeister, L Takacs, H-C Liu, W Gu, M. Sienkiewicz, R.D. Koster, R. Gelaro, I. Stajner, and E. Nielsen (2008), The GEOS-5 Data Assimilation System--Documentation of Version 5.0.1, 5.1.0, and 5.2.0. NASA/TM-2007-104606, 27, 1-118.

Rienecker, M.M., and Co-authors (2011), MERRA: NASA's Modern-Era Retrospective Analysis for Research and Applications. *J. Climate*, 24, 3624–3648. doi:http://dx.doi.org/10.1175/JCLI-D-11-00015.1

Rienecker, M.M., M.J. Suarez, R. Gelaro, R. Todling, J. Bacmeister, E. Liu, M.G. Bosilovich, S.D. Schubert, L. Takacs, G.-K. Kim, S. Bloom, J. Chen, D. Collins, A. Conaty, A. da Silva, et al. (2011), MERRA: NASA's Modern-Era Retrospective Analysis for Research and Applications. *J. Climate*, 24, 3624-3648, doi: 10.1175/JCLI-D-11-00015.1.

Shapiro, S.S., and M.B. Wilk (1965), An analysis of variance test for normality (complete samples). Biometrika, 52, 591 – 611, doi:10.1093/biomet/52.3-4.591.

Sharma, A.R., S.K. Kharol, K.V.S. Badarinath, and D. Singh (2010), Impact of agriculture crop residue burning on atmospheric aerosol loading – a study over Punjab State, India, *Ann. Geophys.*, 28, 367–379, doi:10.5194/angeo-28-367-2010.

Tripathi, S.N., S. Day, A. Chandel, S. Srivastava, R.P. Singh, and B. Holben (2005), Comparison of MODIS and AERONET derived aerosol optical depth over the Ganga basin, India. *Ann. Geophys.*, 23, 1093-1101, doi:10.5194/angeo-23-1093-2005.

U.S. Census Bureau http://www.census.gov/ipc/www/idb/

Venkataraman, C., G. Habib, D. Kadamba, M. Shrivastava, J.-F., Leon, B. Crouzille, O. Boucher, D. Streets (2006), Emissions from open biomass burning in India: Integrating the inventory approach with high-resolution Moderate Resolution Imaging Spectroradiometer (MODIS) active-fire and land cover data. *Global Biogeochem. Cycles*, 20, GB2013, doi:10.1029/2005GB002547.

Vinoj, V., S.S. Babu, S.K. Satheesh, K.K. Moorthy, and Y.J. Kaufman (2004), Radiative forcing by aerosols over the Bay of Bengal region derived from shipborne, island-based, and satellite (Moderate-Resolution Imaging Spectroradiometer) observations. *J. Geophys. Res.*, 109, D05203, doi:10.1029/2003JD004329.

Wu, W.S., R.J. Purser, and D.F. Parrish (2002): Three-dimensional variational analysis with spatially inhomogeneous covariances. *Mon. Weather. Rev.*, 130, 2905–2916, doi:http://dx.doi.org/10.1175/1520-0493.

Zhang, J. and J.S. Reid (2006), MODIS Aerosol Product Analysis for Data Assimilation: Assessment of Over-Ocean Level 2 Aerosol Optical Thickness Retrievals. *J. Geophys. Res.*, 111(D22), D22207. doi:10.1029/2005JD006898.

Zhang, J.L. and J.S. Reid (2010), A decadal regional and global trend analysis of the aerosol optical depth using a data-assimilation grade over-water MODIS and Level 2 MISR aerosol products. *Atmos. Chem. Phys*., 10, 10949-10963, doi:10.5194/acp-10-10949-2010.

Zhao, T. X.-P., I. Laszlo, W. Guo, A. Heidinger, C. Cao, A. Jelenak, D. Tarpley, and J. Sullivan (2008), Study of long-term trend in aerosol optical thickness observed from operational AVHRR satellite instrument, J. Geophys. Res., 113, D07201, doi:10.1029/2007JD009061.

Acknowledgements We gratefully acknowledge the GES-DISC Interactive Online Visualization and Analysis Infrastructure (Giovanni) for providing us with TRMM data.

Table 1. The overview of main attributes of NASA MERRAero assimilated aerosol data.

Feature	Description
Model	GEOS-5 Earth Modeling System (with GOCART aerosol components); Constrained by MERRA Meteorology (Replay) Land sees obs. precipitation (like MERRA*Land*) Driven by QFED daily Biomass Emissions
Aerosol data assimilation	Local Displacement Ensembles (LDE) MODIS reflectances AERONET Calibrated AOT's (Neural Net) Stringent cloud screening
Period	mid 2002-present (Aqua + Terra)
Resolution	Horizontal: nominally 50 km Vertical: 72 layers, top ~85 km
Aerosol Species	Dust, sea-salt, sulfates, organic & black carbon

Table 2. Eight-year (2002-2009) mean AOT (τ), standard deviation (sd), and AOT slope (α) of MERRAero AOT averaged over the specified zones in October[υ].

Area	Zone #	Geographic Coordinates	τ	sd	α (per year)	S – W test	p
IS	1	28.5N – 31.5N 72.7E – 75.7E	0.53	0.07	-0.005	Normal	Not significant
	2	27N – 30N 75.7E – 78.7E	0.50	0.08	-0.004	Normal	Not significant
	3	25N – 28N 78.7E–81.7E	0.51	0.08	0.008	Normal	Not significant
	4	24N – 27N 82.5E–85.5E	0.43	0.05	0.012	Normal	Not significant
	5	22N – 25N 86E – 89E	0.35	0.05	0.010	Normal	Not significant
BoB	6	18N – 21N 87E – 90E	0.22	0.05	0.015	Normal	0.043
	7	15N – 18N 84E – 87E	0.20	0.05	0.020	Normal	0.006

[υ]The decision based on the Shapiro – Wilk normality test for residuals (S-W test) and the significance level (p) are also displayed. If the p value was too high as compared with the 0.05 significance level, the obtained linear fit was considered as statistically insignificant.

Table 3. The eight-year mean AOT (τ), standard deviation (sd), and AOT slope (α) for long-term changes of MERRAero AOT for different aerosol species (desert dust; organic and black carbon; and sulfates) averaged over specified zones in October. F corresponds to the fraction of aerosol component AOT (in percentages) from the total MERRAero AOT.

Area	Zone #	F %	τ	sd	α (per year)	S – W test	p
					Sulfates		
IS	1	31.7	0.17	0.04	0.001	Normal	Not significant
	2	36.7	0.18	0.04	-0.001	Normal	Not significant
	3	43.7	0.22	0.05	0.004	Normal	Not significant
	4	49.7	0.22	0.04	0.006	Normal	Not significant
	5	55.9	0.20	0.03	0.004	Normal	Not significant
BoB	6	52.9	0.12	0.03	0.008	Normal	0.050
	7	50.7	0.10	0.03	0.011	Normal	0.004
					Organic and black carbon		
IS	1	37.7	0.20	0.05	-0.011	Normal	Not significant
	2	39.2	0.20	0.03	-0.009	Normal	Not significant
	3	37.7	0.19	0.02	-0.001	Normal	Not significant
	4	37.5	0.16	0.02	0.002	Normal	Not significant
	5	34.9	0.12	0.02	0.003	Normal	Not significant
BoB	6	28.8	0.06	0.02	0.004	Normal	Not significant
	7	25.9	0.05	0.02	0.005	Normal	0.026
					Desert dust		
IS	1	29.5	0.16	0.04	0.006	Normal	Not significant
	2	23.2	0.12	0.03	0.006	Normal	Not significant
	3	17.8	0.09	0.03	0.005	Normal	Not significant
	4	12.2	0.05	0.02	0.004	Normal	Not significant
	5	8.0	0.03	0.01	0.004	Normal	0.035
BoB	6	8.3	0.02	0.01	0.004	Normal	0.012
	7	8.1	0.02	0.01	0.004	Normal	0.008

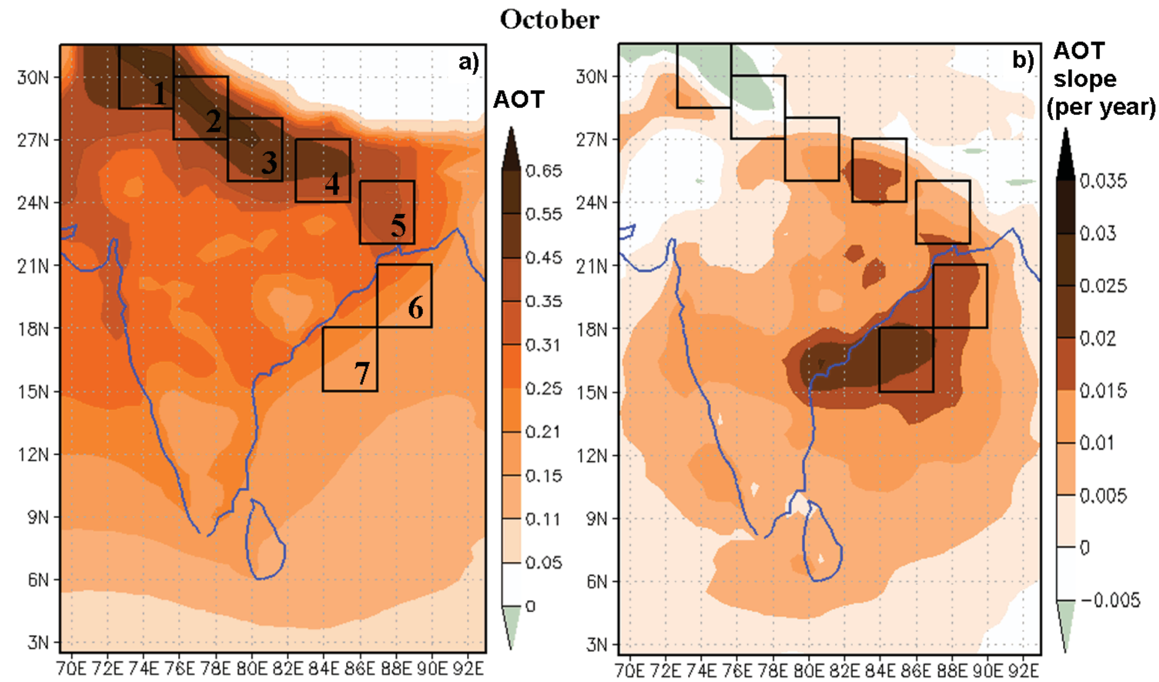

Figure 1. Spatial distributions of (a) the eight year (2002 – 2009) mean MERRAero AOT and (b) its trends (characterized by AOT slopes) in October. The AOT trend values correspond to the slope of the linear regression analysis. The squares show the locations of zones 1 to 7 within the study region.

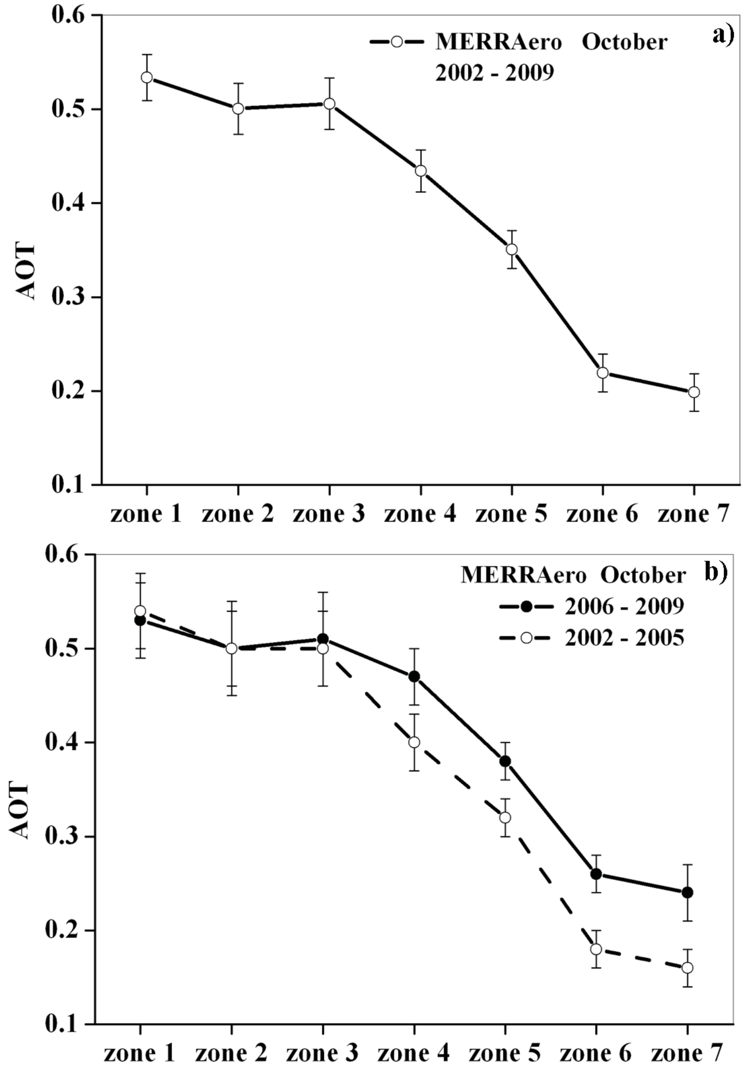

Figure 2. a - zone-to-zone variations of eight-year (2002-2009) mean MERRAero AOT averaged over the specified zones. b - zone-to-zone variations of MERRAero AOT averaged over the first four-year (2002-2005) period and over the second four-year (2006-2009) period. The error bars show the standard error of mean AOT.

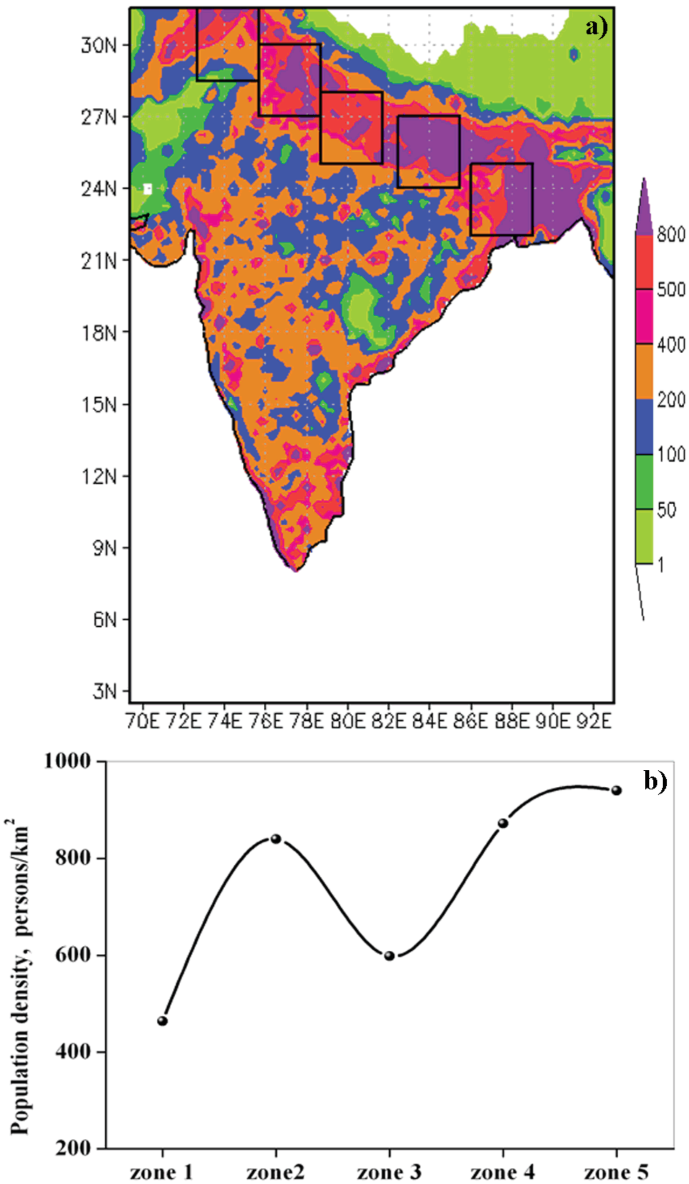

Figure 3. a – population density (persons km^{-2}) distributions over the Indian subcontinent. b – zone-to-zone variations of population density averaged over the specified zones. The GPW-v3 gridded population density data for the year 2005 were used (http://sedac.ciesin.columbia.edu/data/collection/gpw-v3).

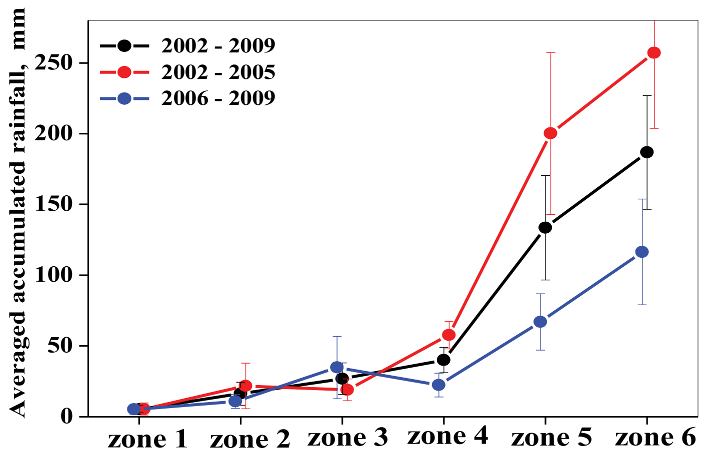

Figure 4. Zone-to-zone variations of TRMM accumulated rainfall over the specified zones in October averaged over the eight-year study period (2002 – 2009), over the first 4-year period (2002 – 2005), and over the second 4-year period (2002 – 2009). The error bars show the standard error of mean accumulated rainfall. TRMM data from the 3B42V6 archive were used.

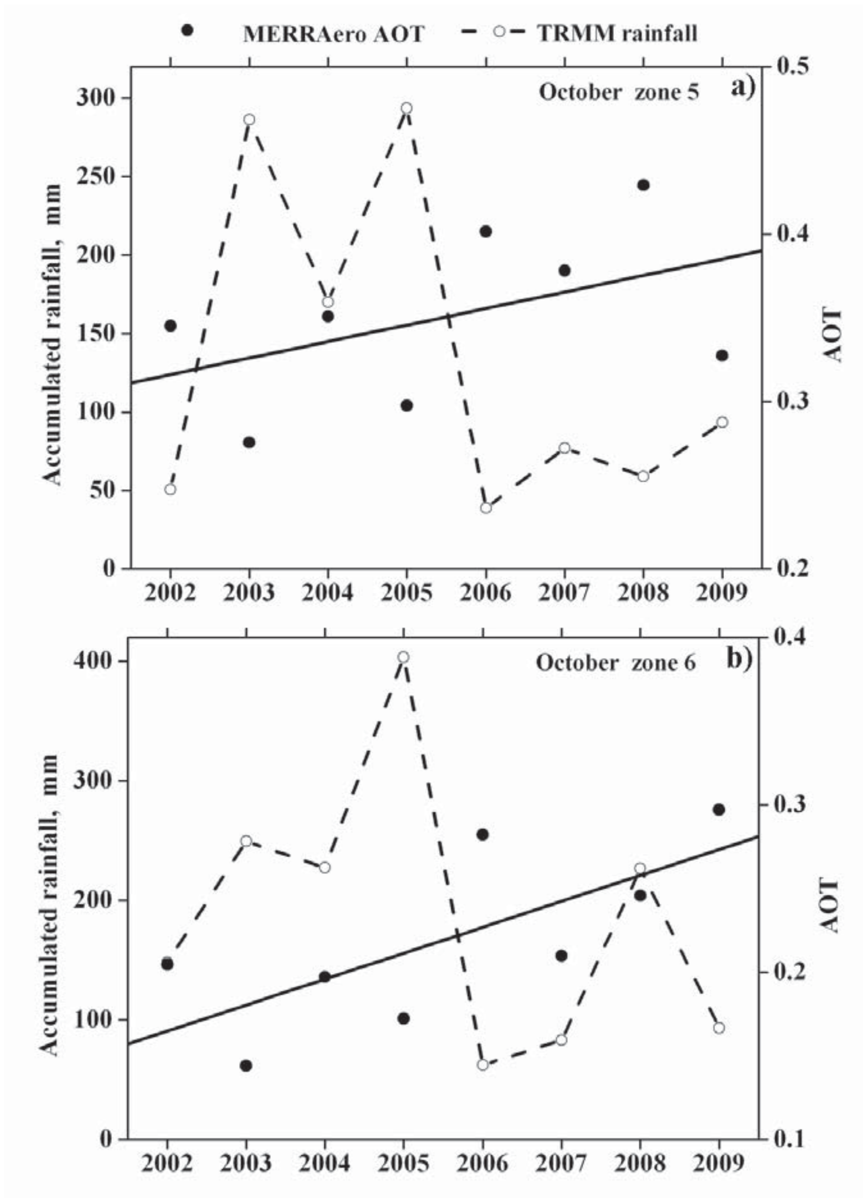

Fig. 5. Year-to-year variations of MERRAero AOT and TRMM rainfall over (a) the east of the Ganges basin (zone 5) and (b) north-west BoB (zone 6) in each October during the study period. TRMM rainfall data from the 3B42V6 archive were used. The straight solid lines designate linear fits.

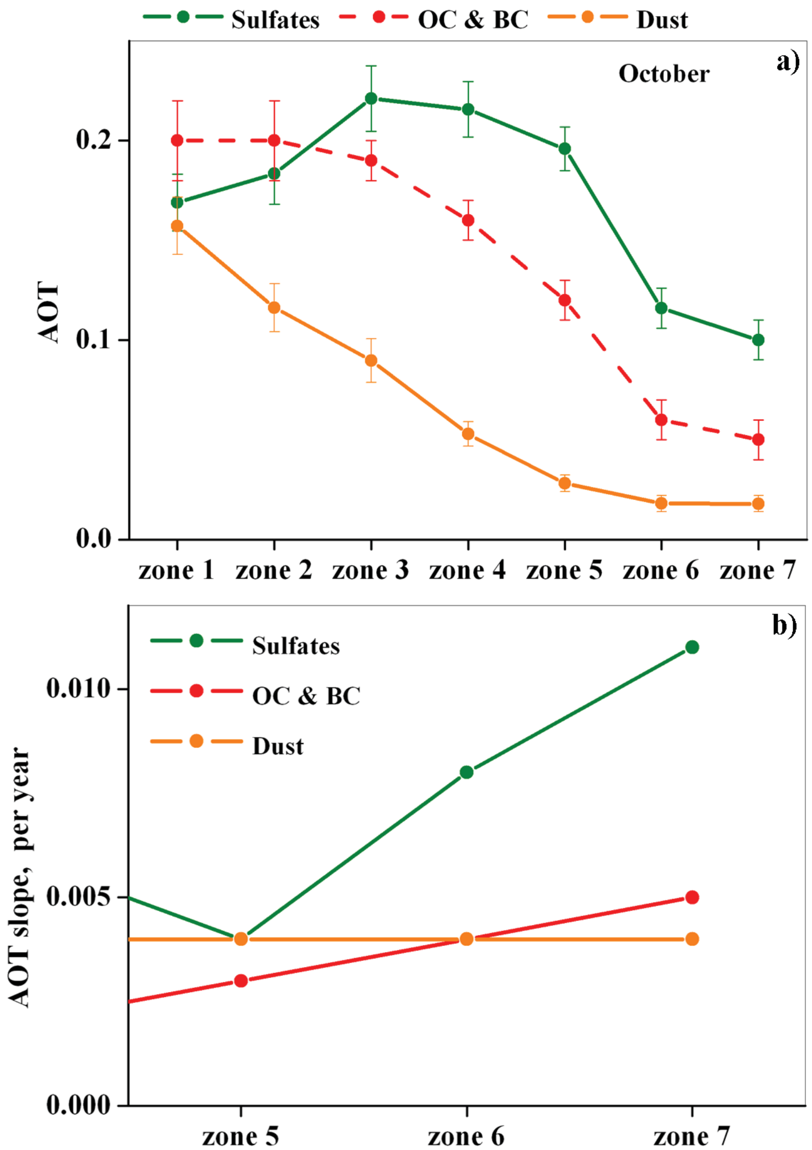

Figure 6. Zone-to-zone variations of (a) eight-year (2002-2009) mean MERRA AOT of different aerosol components (sulfates (SU), organic and black carbon (OC & BC), and desert dust) averaged over the specified zones in October, and (b) their AOT trends (characterized by the slope of the linear regression analysis). The error bars show the standard error of mean AOT.

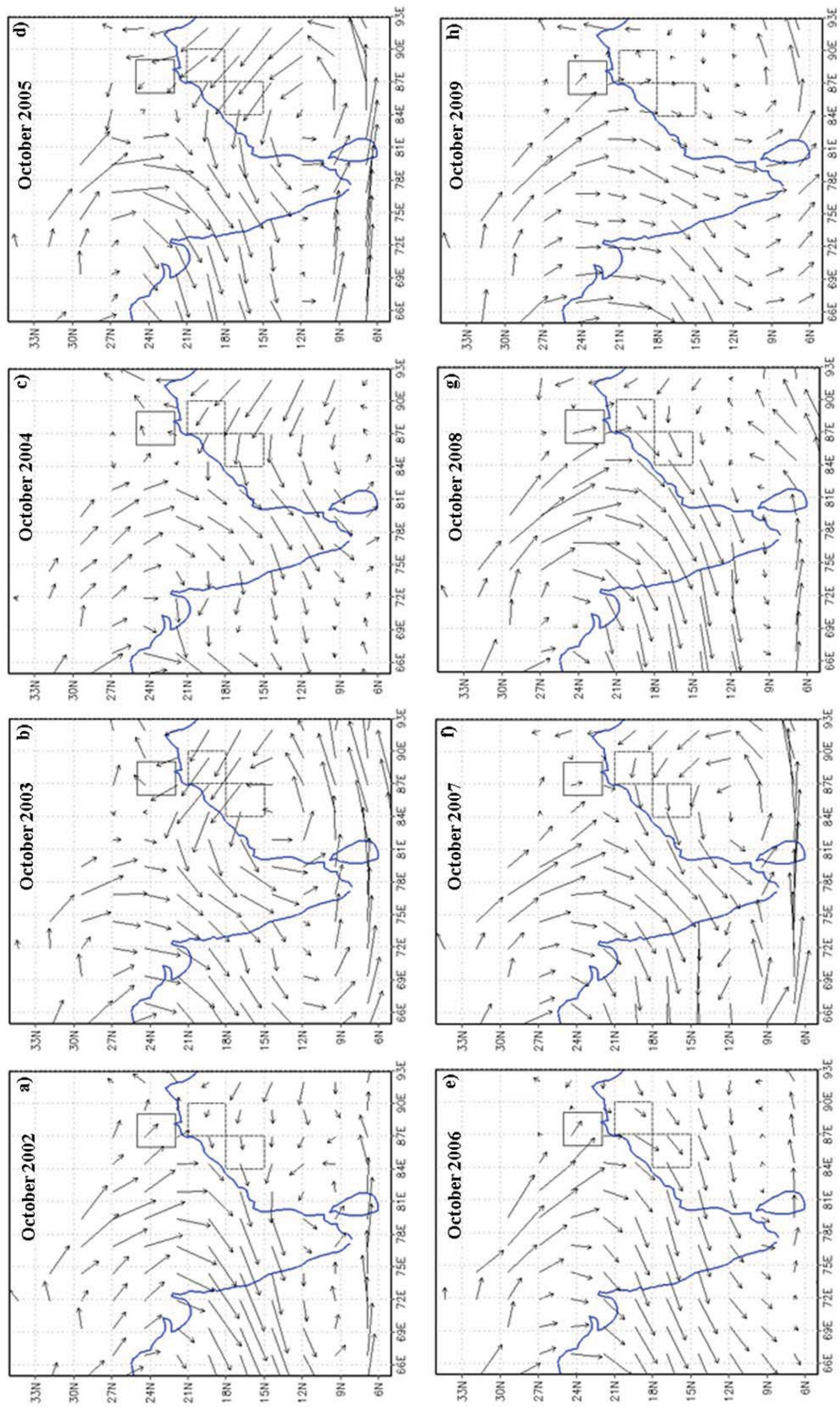

Figure 7. Spatial distributions of mean MERRA wind vectors of the 700-850 hPa layer in each October during the study period.

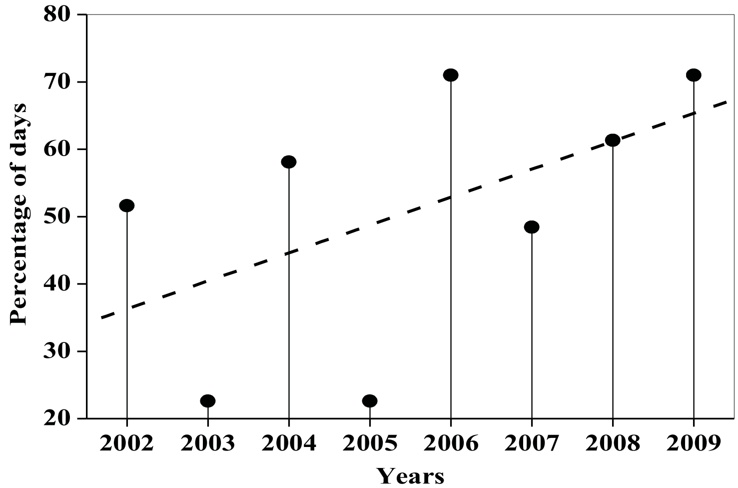

Figure 8. Numbers of days (in percentage form) in each October during the study period when prevailing wind (transporting air pollution) blew from the east of the Ganges basin (zone 5) to north-west BoB (zone 6). The straight dashed line designates a linear fit.

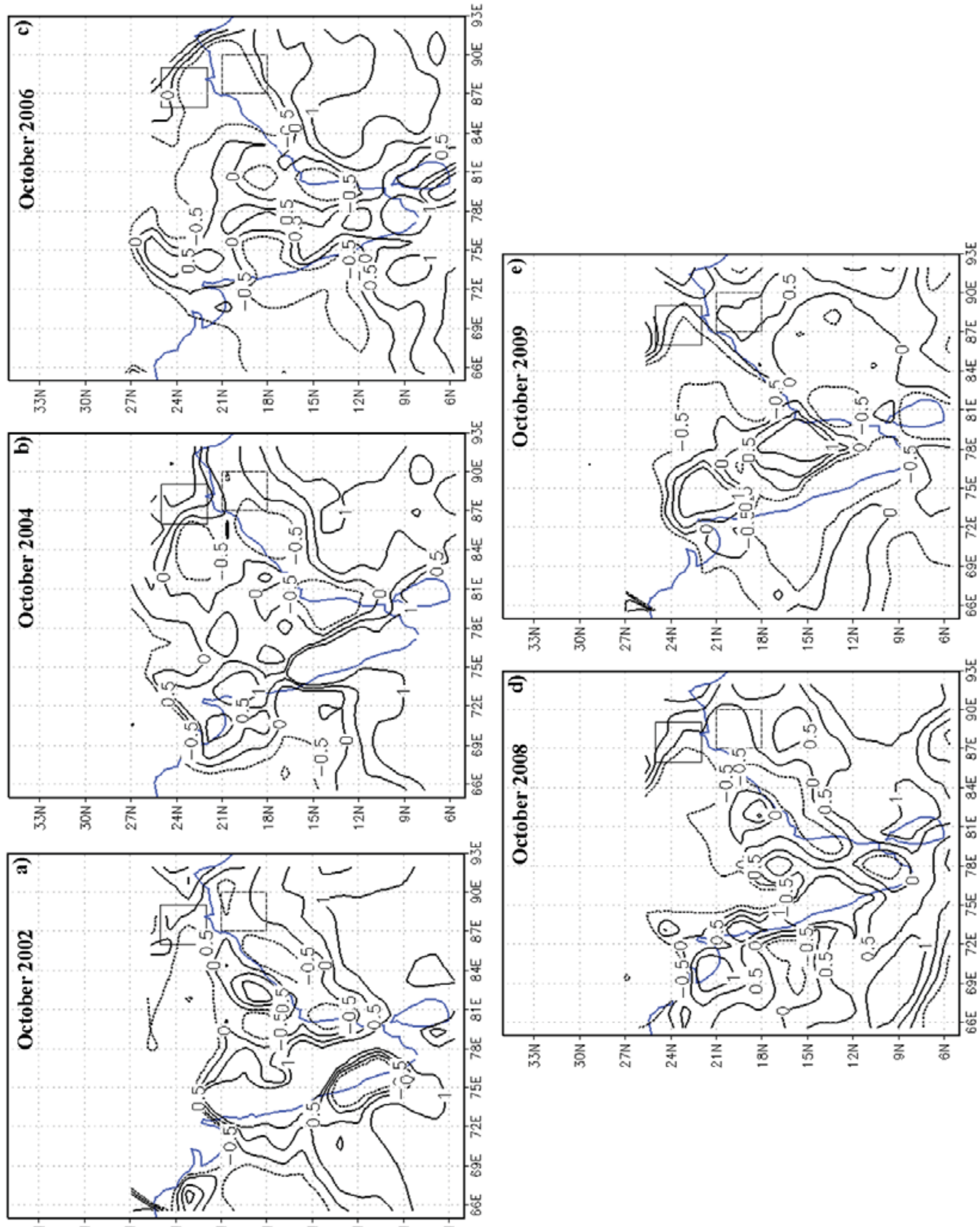

Figure 9. Spatial distributions of mean wind convergence (10^{-6} s^{-1}) of the 700-850 hPa layer for each October, when the number of days with prevailing winds, blowing from the east of the Ganges basin (zone 5) to north-west BoB (zone 6), exceeded 50%. MERRA wind reanalysis data were used.

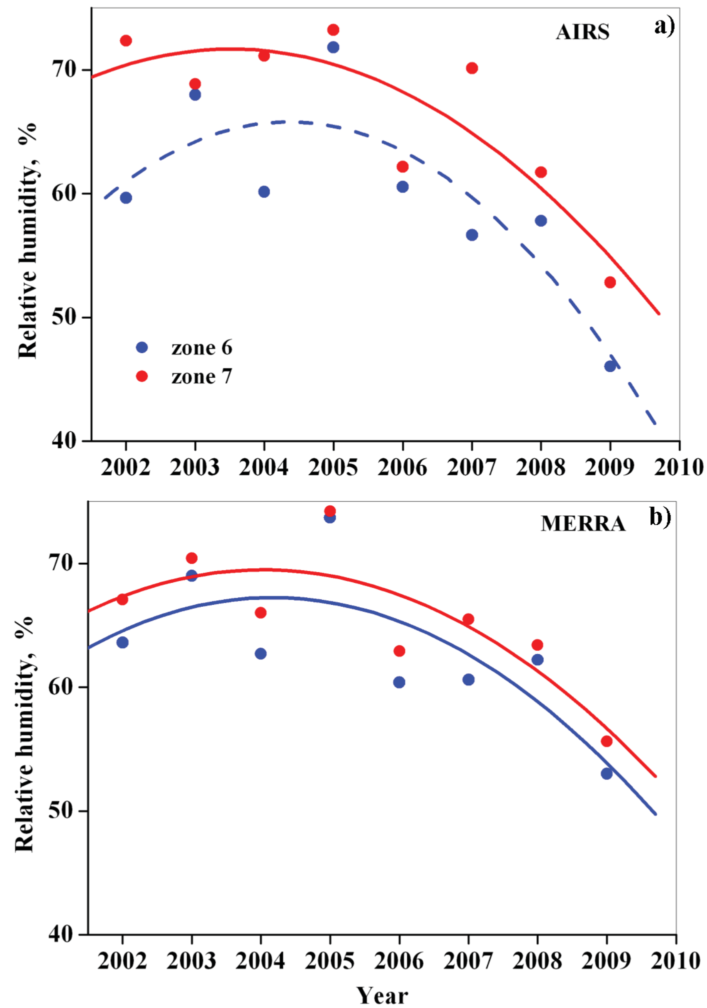

Figure 10. Year-to-year variations of relative humidity (RH) of the 700-850 hPa layer in each October during the study period based on (a) AIRS monthly data (taken on the descending node of the orbit, on the day side of the Earth), and (b) the MERRA monthly data.

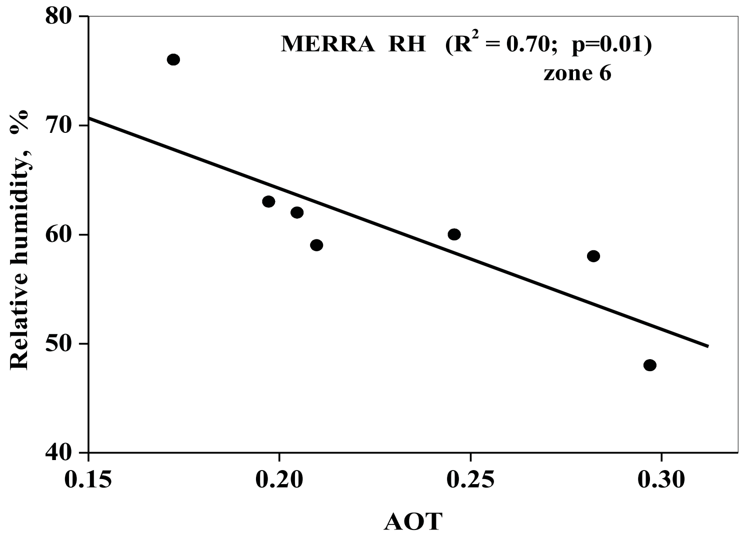

Figure 11. Scatter-plot between monthly MERRA relative humidity of the 700-850 hPa layer and MERRAero AOT over north-west BoB (zone 6) in each October during the study period. The straight line designates a linear fit.